Gas Mapping LiDAR Aerial Verification Program Final Report

Alberta Upstream Petroleum Research Fund Project 17-ARPC-03

Written by

Doug Hunter, VP Systems R&D,
LiDAR Services International Inc.
and
Mike Thorpe, PhD, CTO,
Bridger Photonics Ltd.

EXECUTIVE SUMMARY

The oil & gas industry and the environmental community are specifically considered by this report, which introduces and evaluates the Bridger Photonics Airborne Gas Mapping LiDAR (GML) sensor. GML is a Light Detection And Ranging (LiDAR) sensor that performs remote measurements of methane gas concentrations, methane emission rates and 3D terrain topography from an aircraft platform, helicopter or fixed wing. GML is intended to be an efficient and cost effective tool for detecting, quantifying and prioritizing the repair and/or mitigation of methane leaks over large geographic areas. This report summarizes the results of the first flight tests performed with the GML from a fixed wing aircraft, conducted in September 2017.

These tests, sponsored by the Petroleum Technology Association of Canada (PTAC) and the Alberta Upstream Petroleum Research Fund (AUPRF), successfully demonstrated the effectiveness of the GML sensor. The data reflects its scientific and field operations capabilities for comprehensive identification, visualization and reporting of methane emissions 1 m^3/day and larger.

Summaries of the objectives, tests and results of the program follow, as well as LSI's conclusions regarding the optimal and immediate implementation of the sensor for emissions monitoring and mapping.

Table of Contents

1.0 INTRODUCTION

The need for effective methane emissions mapping on an international scale has recently become very apparent and broadly discussed. As an aerial remote sensing company, LSI has been active in pursuing the most effective gas sensor available with the premise that "what gets measured well can be managed well". Airborne remote sensing provides a unique opportunity for the collection of appropriate coordinated datasets as part of the global tool set for leak and emissions prevention, detection and remediation. The effectiveness of any emissions mapping for collecting rapid, accurate and economical data is totally dependent on the right sensor and the right platform being implemented.

LSI believes the Bridger Photonics GML sensor technology is extremely well-suited for emissions mapping and leak detection based on the understanding that it is:

- An active rather than passive sensor – no dependence on and little detrimental effects from ambient light conditions.
- Able to be flown at safe altitudes above the ground and hence not compromised by potentially dangerous gas plumes, above ground obstacles and civil airspace restrictions.
- Capable of precise leak concentration and plume definition as well as broad area coverage during flight.
- Rapid in collection speed and capable of being used for long endurance missions resulting in maximum coverage.
- As economical as possible while still providing high quality results.
- Able to minimize the possibility of false positives detection and missed positives (Type 1 and Type 2 error reduction), and if emissions are present they will be detected, quantified and reported.
- Able to accurately geo-reference all results, whereby data can be readily integrated into clients' GIS systems and operational databases.

It is hoped that this study will demonstrate the applicability of the Gas Mapping LiDAR sensor for use in Canadian Oil and Gas operations.

2.0 GOALS

The specific goals of this project are:

- To engage in the airborne measurement of controlled emissions releases at variable volume rates to verify and quantify the GML sensor's functionality for gas concentration and gas flux rate measurements.

- To extend the controlled tests to include the identification and measurement of uncontrolled releases at operating oil and gas facilities.

- To successfully install and operate the sensor in an aircraft to verify its functionality in a real operations environment and to determine what measures/improvements need to be undertaken to make it fieldworthy.

- To determine what effort is needed to integrate the sensor and its data into a proven airborne survey navigation and data collection system, and to confirm its integration with geomatics operations procedures and methodologies.

- To determine the best methods for data and imagery analysis and delivery of the results to end users.

- To determine if the 3D capability of the ranging aspect of the Gas Mapping LiDAR sensor is effective for coincident 3D feature mapping while engaging in gas emissions surveys.

- To determine the next steps for industry application and commercialization.

The overarching goal is that this project will provide physical and scientific verification of the GML sensor and system in a real operations environment.

3.0 THE SYSTEM

3.1 The Aircraft

The aircraft used for GML flight testing was the Pipistrel Virus SW1, operated by Darryl Zubot of Z-Air. The Pipistrel is a light weight and highly-efficient carbon fiber aircraft with long flight endurance and two seats, one for the pilot and the other occupied by the GML operator. The Pipistrel is outfitted with a sensor port that was used to mount Bridger's Gas Mapping LiDAR sensor using a custom-milled aluminum mount and mounting plate, fabricated by LiDAR Services International, according to Bridger specifications. The GML's GPS antenna was mounted inside the Pipistrel cockpit, near the top of the front windshield, where it had sufficient view of the sky to acquire signals from 12 or more GNSS satellites at any time. A power inverter onboard the Pipistrel was used to provide the GML with the required 28 V power supply. Sensor operation and data logging were controlled by the GML operator, through a laptop in the aircraft. Survey navigation information, defined during mission planning, was entered and managed through the aircraft's internal flight management system. Integration of the GML sensor onto the Pipistrel, preliminary testing of the equipment on the ground and the first two facility scans were performed on the first day of the project. In **Figure 1** below, the GML sensor assembly is visible mounted underneath the Pipistrel fuselage, behind the forward landing gear.

Figure 1. Gas Mapping LiDAR Sensor mounted on the Pipistrel Aircraft.

3.2 The Sensor

The GML is an airborne Light Detection And Ranging (LiDAR) sensor that performs remote measurements of methane gas concentration and the distance to physical objects (e.g. the ground, vegetation, infrastructure, etc.). The GML consists of four primary sensors: a spatially-scanned range finding laser, a spatially-scanned gas absorption laser, an colour frame camera and a Global Navigation Satellite System-Inertial Navigation System (GNSS-INS). Bridger combines the sensor outputs in software to provide geo-registered data that includes gas plume imagery, 3D point cloud and orthorectified RGB imagery. The term geo-registered means that a set of geographic coordinates and the measurement time is associated with each gas, camera image and 3D point cloud measurement. The range finding and gas sensing lasers are co-aligned and are scanned in a roughly circular pattern as the aircraft flies along its trajectory to provide coverage of a swath of terrain below the aircraft. The point density on the ground depends on flight altitude and flight speed. For example, at low flight speed and altitude (80 kph and 100 m) the point densities are 29 points/m^2 for range and 14 points/m^2 for gas, whereas for high flight speed and altitude (180 kph and 210 m) the point densities are 6 points/m^2 for range and 3 points/m^2 for gas. The methane sensing laser is used to perform wavelength modulation spectroscopy (WMS) integrated-path gas absorption measurements.[i] This means the integrated methane concentration between the sensor and the backscatter target (e.g. the ground, etc.) is the quantity being measured. Integrated-path absorption has physical units of concentration times length and is typically reported in units of parts-per-million times meters (i.e. ppm-m). The range measurement laser is used to measure the distance from the sensor to the backscatter target. The range information is used to create topographic maps of the backscatter target topography (ground, vegetation, infrastructure, etc.) within the measurement swath.

Parameter	Performance
Max measurement distance	230 m
Measurements per second	10,000
Field of View	18°
Concentration detection limit	10-15,000 ppm-m (CH_4)
Minimum detectable leak rate (1 m/s wind, 5σ, @max altitude)	10 lpm
Range Precision (1σ)	0.2 m
SW&P	12”x14”x20”, 21 kg, 150 W
Ingress protection/Impact rating	IP54
Operating temperature range	10 °C – 40 °C

Figure 2. Left: GML mounted on the Pipistrel Virus SW1 during a flight test near Edmonton, AB. Right: Performance specifications of the prototype GML used for the testing described herein. Production GML sensors will have improved performance in nearly all areas, see Section 7 for details.

An image of the prototype GML sensor used to perform the flight tests described in this report and a table of its performance specifications are shown in Figure 2.

The GML is powered by 28 VDC provided by an inverter onboard the aircraft, and is controlled via laptop computer by an operator occupying the passenger seat of the Pipistrel. Additionally, a GPS antenna is mounted inside the cockpit to receive satellite signals used by the GML’s onboard navigation system. Three electrical cables pass from the Pipistrel cockpit to the GML sensor, a power cable that delivers 28 VDC, an Ethernet cable that connects the GML to the laptop computer and a coaxial cable that connects

the GML to the GPS antenna. Gigabit Ethernet communications enable real-time streaming of all GML data from the sensor to the laptop and allows control of all GML functions by the operator. For the prototype GML the data processing was not automated. During the flights the operator periodically processed small segments of the data using Matlab processing scripts to ensure successful data acquisition while still in flight. Bridger is currently working on graphical user interface (GUI) with automated data processing that will enable real-time visualization and quantification of detected leaks without human intervention (see Section 5.3 and Section 7).

3.3 3D Modeling Capability

GML's 3D terrain modeling capability is based on a combination of spatially-scanned LiDAR range data, encoder data from the LiDAR beam scanner and position and orientation data provided by the onboard GNSS-INS. GML range measurements are based on Bridger's frequency-modulated-continuous-wave (FMCW) LiDAR distance measurement technique, illustrated in **Figure 3**.[ii] FMCW distance measurements are performed by splitting the output of a frequency-chirped laser into two portions. One portion is transmitted to a remote target and the other portion is kept locally, inside the GML. A receiver collects light backscattered from the remote target and interferometrically combines it with the portion of the laser beam kept locally. The combined beam produces an oscillating 'beat' signal with frequency (f_{beat}) that is proportional to the target distance. FMCW distance measurements have several benefits compared to other laser range finding measurements including better distance resolution for distinguishing closely spaced objects and better dynamic range for reliably detecting both high reflectivity and low reflectivity targets.

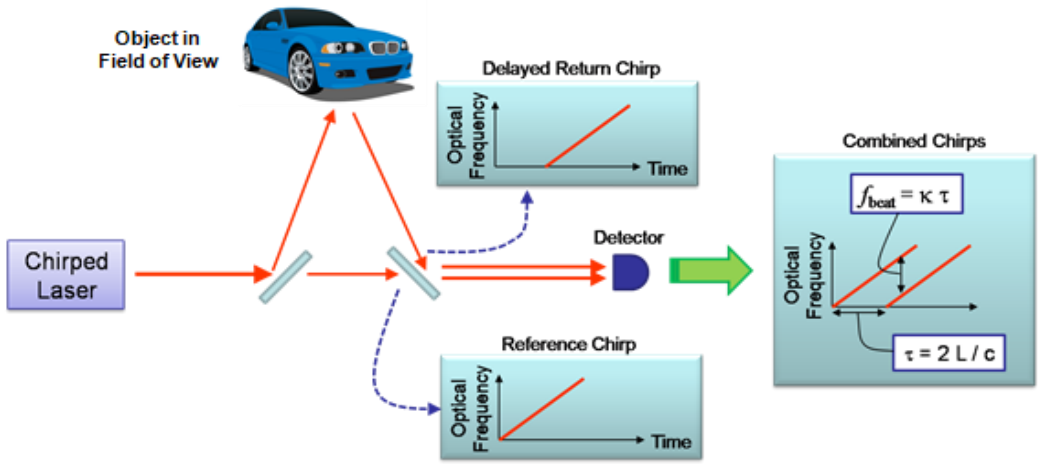

Figure 3. Schematic of the FMCW distance measurement technique.

A geo-registered point cloud of objects within the measurement swath is then produced by combining a set of spatially-scanned FMCW range measurements with angle encoder measurements from the LiDAR beam scanner and position and orientation measurements for the GNSS-INS. The beam scanner encoder data provides information regarding the direction of the transmitted LiDAR beam relative to the GML sensor for each FMCW range measurement. The position and orientation data from the GNSS-INS provides information about the geographic location and sensor orientation for each FMCW range measurement. Combining these pieces of information allows for computation of the geographic location of each backscatter target detected by the FMCW range measurements. The resulting set of point cloud data is referred to as a geo-registered 3D point cloud. Geo-registered gas concentration and RGB camera measurements are produced using a similar procedure. The geo-registered 3D point cloud data can be further processed to extract useful information, such as distinguishing the ground from above ground

objects, definition of the ground height and measuring the physical dimensions of terrain and infrastructure features.

While the Bridger GML sensor's primary capability is for methane plume imaging it is also, by its very nature as an advanced laser-based LiDAR instrument, capable of 3D terrain modelling. Samples of the coincident ranging information collected during these test flights were analyzed by LiDAR Services International using standard LiDAR processing routines. This basic LiDAR mapping processing included the "ground surface extraction" and the "above ground feature classification", or in other words, the DEM (Digital Elevation Model) and infrastructure modeling.

Standard LiDAR mapping processes were used to locate overlapping point differences between scan lines, and it was noted that these could be used in a temporal data analysis for change detection of physical features. This change detection aspect could be used in facility and Right Of Way modeling and management. It would require some technical advancements be implemented within the sensor to improve the quality and accuracy of the 3D point data as Bridger themselves have suggested, and these are expected to provide new value-added mapping capabilities in the near future. For instance, these terrain modelling advancements would be automatically generated for areas of interest related to the terrain surrounding reported anomalies. Thus, providing much more data than the present visual inspection aerial reporting for ground crew access, hazards, vegetation and so on.

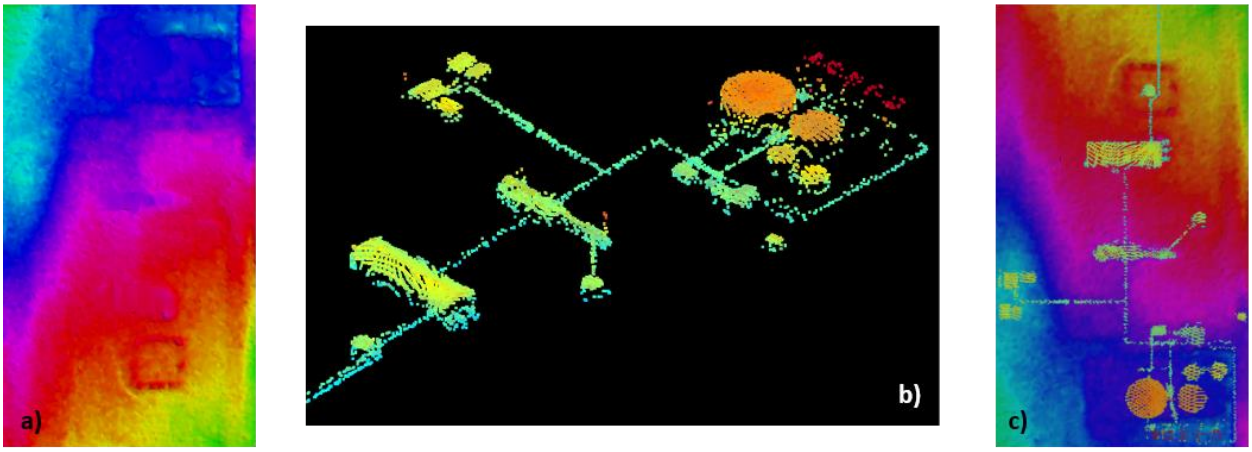

Figure 4. 3D Terrain and Feature Modelling Examples: a) Digital Elevation Model (DEM) showing bare Earth topography, b) Above ground features e.g. buildings and infrastructure, c) Derived Features Model.

3.4 GIS-Driven Data Management and Delivery

An important part of our commercialization plan includes an already-established capacity to organize and warehouse geo-referenced data. LSI has developed a GIS-driven web application (ReGIS) that provides secured raw GIS data access. ReGIS also provides quick and easy browsing of data via an online map interface. With sufficient data, ReGIS can ultimately illustrate temporal fluctuations and be used to conduct progressively intelligent analyses. Since ReGIS internally leverages OGC GIS standards, customers can easily interface with their own pre-existing GIS systems, as desired. This provides a standard GIS interface in a simple, standalone package. It is intended to be the initial delivery system for GML data collected during LSI operations. Other GIS packages such as qGIS and ArcGIS and so on, will be seamlessly served by this technique.

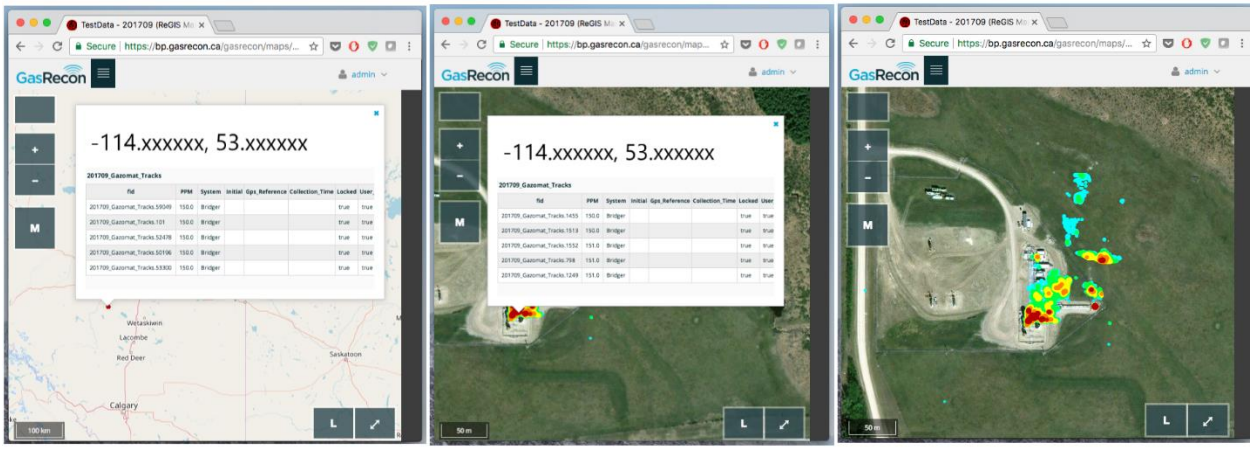

Figure 5. Data management using Gas Recon's ReGIS application.

Figure 5 above illustrates the ReGIS web application's map viewer which has mixed format map source data with overlaid GML data. The ReGIS platform integrates a highly configurable style engine (via Geoserver) which could ultimately be used to create custom reports and search-driven analyses. The images in the centre and towards the left also illustrate "pop-up clouds" which give direct access to raw data as well as non-GIS records.

3.5 Concentration Maps

Methane concentration maps are formed by projecting the path-integrated concentration measurements onto the backscatter target to form a 2D map of gas concentration plume within the swath of terrain covered by the GML field of view. Depending on the flight parameters (altitude and speed) gas concentration images have pixel resolution between 1 m^2 to 2 m^2. A data filtering algorithms are applied to the gas concentration data to produce high-confidence detections of anomalous gas concentrations with high-sensitivity and low occurrences of false positives. A complete plume image of the anomalous gas within the measurement swath is acquired for each fly over.

3.6 Flux Quantification

Flux quantification is performed by combining the methane concentration data and wind speed information. The gas flux (Φ) can be computed by combining the gas concentration (C) and wind speed (u) in a manner similar to the description provided in Ref [iii] using the GML sensor to acquire the path-integrated gas concentration measurements. For the controlled release tests presented herein the wind data was acquired using a local anemometer. For the uncontrolled leaks measured at the oil production facilities wind data for each site was acquired via anemometer for the site 12-31 data capture on 9/12, and from the Meteoblue website for all other facility scans.[iv] The uncertainty in flux estimates (σ_Φ) is related to the uncertainty in the gas concentration σ_C and the uncertainty in the wind speed (σ_u) by $\sigma_\Phi = \sqrt{(\Phi\sigma_u)^2 + (u\sigma_C)^2}$. One or more flux estimates can be produced from a single flight pass. Additional flight passes may be used to improve the accuracy of the flux estimate for a detected leak. See Section 5.1 for controlled release test results.

3.7 Controlled Leak Instrumentation

Controlled methane emission rates were produced using a tank of pure methane from Air Liquide (255 SCF at >99% purity) and a mass flow controller from Alicat Scientific (model MCR-250SLPM-D), see **Figure 6**. The mass flow controller uses active feedback to maintain the methane emission rate at a programmed value between 1 lpm and 250 lpm, with a factory calibrated accuracy defined by (0.8% of reading + 0.2% of full scale). The emission source was a 3/8" inner diameter tube at an above ground height of 1.35m.

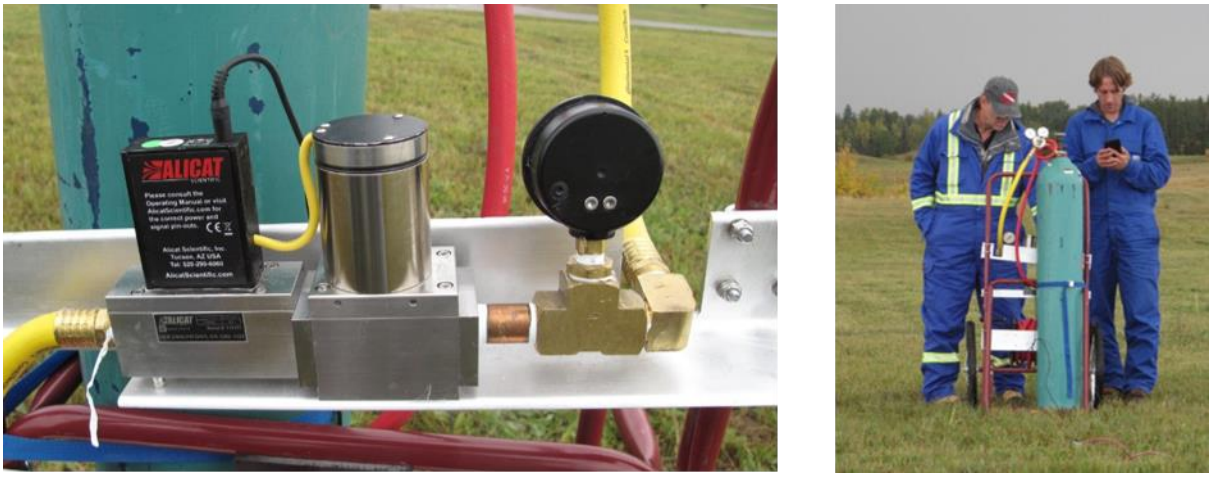

Figure 6. Controlled methane release equipment.

Local wind measurements were performed using an Onset HOBO directional anemometer (S-WCF-M003) that provides wind speed and direction with resolution (0.5 m/s and 1 degree) and accuracy (±1.1 m/s and ± 7 degrees). The anemometer was positioned approximately 20m from the emission source at a height

Figure 7. Controlled methane release test setup at Cooking Lake Site.

of 1.6m above ground. An empirical wind profile was used to convert the wind speed measured by the anemometer to an estimate of the wind speed at the height of the emission source. A secondary anemometer, a research-grade Decagon DS-2 Sonic Anemometer, was also set up for data corroboration and back up, see **Figure 7**. A survey-grade GPS receiver (NovAtel Propak6) was set up at each site for positioning verification and to reduce the errors of the recorded GPS position of the aircraft through post-processed differential correction.

4.0 THE STUDY

4.1 Test Area

LSI and Bridger personnel worked with AER (Alberta Energy Regulator) to select the best area and facilities within that area for the aerial testing program. The optimal zone was selected in the area east of Drayton Valley where multiple, cooperating facilities were within reasonable distances of the Cooking Lake airport, where the aircraft, owned and operated by Z-Air Services is based. Of an initial six facility site prospects, three were selected and flown (12-31, 8-2 and 5-30). The initial controlled leak setup was at one of these, Site 12-31, and was later moved to the Cooking Lake Site due to contamination of the releases by nearby facility venting. A satellite map of the Edmonton area is shown in **Figure *8*** with markers indicating the locations of Cooking Lake Airport, the Cooking Lake Site (used for controlled release testing) and the three facility sites (12-31, 8-2 and 5-30). A picture and zoomed in satellite map of each site location is showing in a) thru d).

Figure 8. Gas Mapping LiDAR Testing Area

a) Site 5-30

b) Site 12-31

c) Site 8-2

d) Cooking Lake Site

Figure 2 – Site Photos

4.2 Test Flight Parameters

Flight passes for both the facility scans and the controlled release tests were performed using a figure 8 flight pattern for optimal efficiency. For the facility scans the figure 8 pattern was used to connect offset flight lines passing over the facility area to acquire a complete scan of each facility, see **Figure *9***. For controlled release testing the figure 8 pattern connected a single cross that intersected over the controlled release location, such that each pass could acquire a controlled release plume image. Measurements of the controlled release site and facility sites were flown at two altitudes, 150m (500') and 210m (700') above ground level. All GML measurements reported here were recorded at a speed of 130 km/h (80 mph).

Figure 9. Example facility scan mission plan for Site 12-31. Flight path lines indicated in grey are offset such that successive passes result in coverage of the entire facility.

5.0 RESULTS AND OBSERVATIONS

This section describes the results of the controlled release tests (Section 5.1) and the facility scan tests (Section 5.2), which resulted in the detection of several un-staged and uncontrolled releases.

5.1 Controlled Releases

The controlled release test was performed on 9/14/2017 between 2:00 pm and 4:00 pm MDT in an open field south of Cooking Lake, AB, see Cooking Lake Site in **Figure 8**. Our initial goal for flux testing had been to perform tests under a wide variety of conditions including varying wind speeds, flight speeds and flight altitudes. We were also hoping to test at multiple sites to explore the effects of terrain variation. However, due to poor weather conditions we were only able to conduct a single stepped emission rate flux test. The test consisted of 50 passes over the controlled emission setup at a flight speed of 130 kph and two different flight altitudes, 150 m and 210 m. As previously mentioned, the width of the measurement swath for all passes was governed by the GML field of view, which was 18°. This means that the measurement swath for the 150 m altitude was 48 m, and the swath for the 210 m altitude was 67 m. Due to the prototype GML's narrow measurement swath and navigation issues, such as roll instability of the aircraft, which are described further in Section 5.3, only 28 of the 50 passes successfully captured the controlled release plume. Example data from a single flight pass over the controlled release setup is shown in **Figure 10**. The left side of the figure shows a geo-registered plume image overlaid on a satellite map and displays the measurement swath consisting of a black dot for each LiDAR measurement point. The orange arrow indicates the wind direction measured by the anemometer.

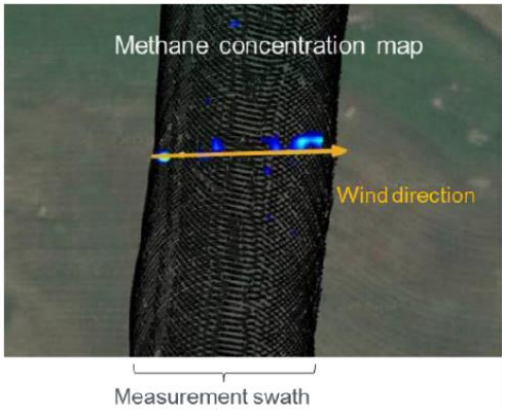

Measurement Parameter	Measurement value
Flight altitude	150 m
Pass number	19
Wind speed	1.2 m/s
Wind direction	96°
Actual emission rate	40 LPM
Measured emission rate	37 LPM

Figure 10. Left: Example data from one of the successful 40 lpm controlled emission rate flight passes. The black dots show the locations of individual LiDAR measurements and the orange arrow indicates the wind direction. Right: The flight altitude and measurement results from the pass shown on the left.

The right side of the figure lists the flight altitude and the measured wind speed, wind direction and methane emission rate for this measurement pass. Controlled release measurements were performed at four different emission rates (10 lpm, 20 lpm, 40 lpm and 60 lpm). Also, before the emission was turned on, several flight passes were performed with no emission present. During the course of this test we experienced winds from all directions and wind speeds ranging from 0 m/s to 1.7 m/s. Example images of

the controlled release plume produced at each emission rate is shown in **Figure 11.** The results for all 28 passes are shown in **Figure 12**. The blue line indicates the prescribed methane flow rate programmed into the mass flow controller for each pass. The red asterisks show the flux estimates that were derived by combining the anemometer wind measurements with the GML methane concentration measurements

Figure 11. Controlled release plume images for the four emission rates. The arrows next to the plume indicate the wind direction and velocity at the time each image was acquired.

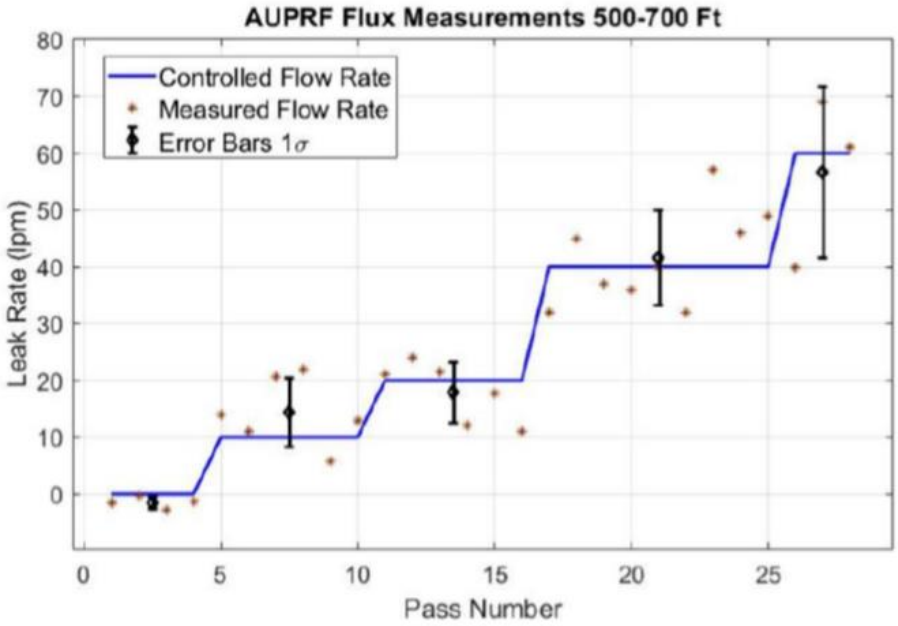

Figure 12. Flux measurement results for 28 successful passes.

for each individual pass. The average flux measurement for each mass flow controller setting is indicated by a black diamond with error bars. Although the statistics, and the environmental conditions, are limited, the data suggests Bridger's approach to flux quantification provides a 1σ accuracy of defined by ±2 lpm ± 40% of the measured value for a single flight pass. The data also suggests that additional passes (i.e. more than a single pass) will increase the flux measurement accuracy. More data will be required to further constrain the measurement accuracy and to determine the optimal number of passes that should be performed in cases where high accuracy is required.

5.2 Facility Releases

Facility scans were performed on 9/12/2017 and 9/14/2017 for the following sites - LSD 8-2, LSD 12-31 and LSD 5-30. A total of five complete facility scans were performed using flight line patterns similar to those shown in **Figure 8**. The time required to scan a facility depends on the facility size. Given the prototype GML field of view (18°) and the nominal flight altitude of 150 m a minimum of three flight passes was required to acquire a complete scan of LSD 8-2. Two compete scans of the LSD 8-2 facility were performed during the test period, one on 9/12/2017 and one on 9/14/2017. A total of 10 flight passes were performed for each scan to ensure complete coverage and to get multiple looks at detected plumes.

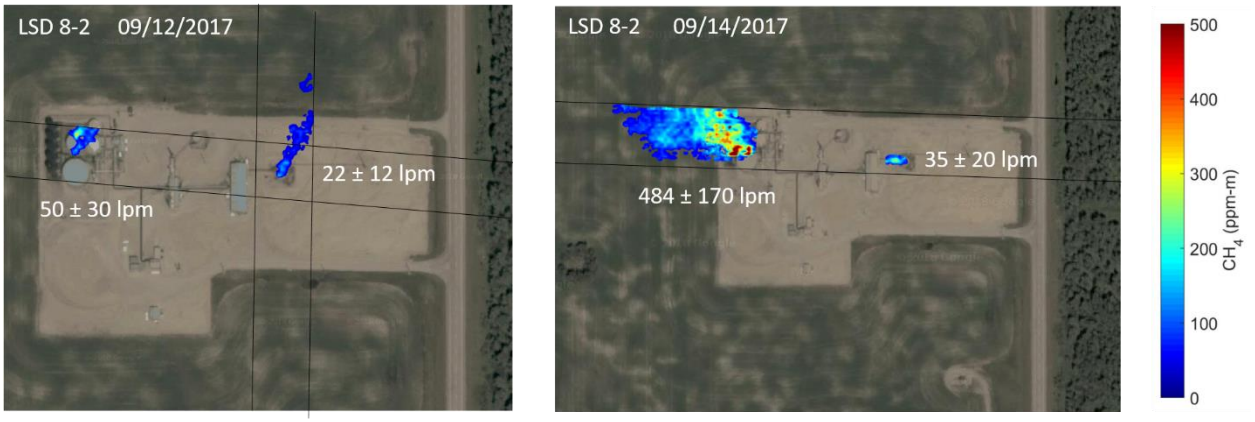

Figure 13. LSD 8-2 facility scan flight passes acquired on 9/12/2017 (left) and 9/14/2017 (right). The black lines indicate the measurement swath for the displayed flight passes, and flux estimates shown next to each detected plume.

Methane concentration images from a few of the flight passes over LSD 8-2 are shown in **Figure 13**. An aggregate image of the gas plumes recorded from all passes may be compiled from the individual flight pass data, an example for LSD 8-2 is shown in **Figure 14**. However, aggregate images may be difficult to interpret as shifts in the wind direction and speed between successive flight passes may cause unrealistic

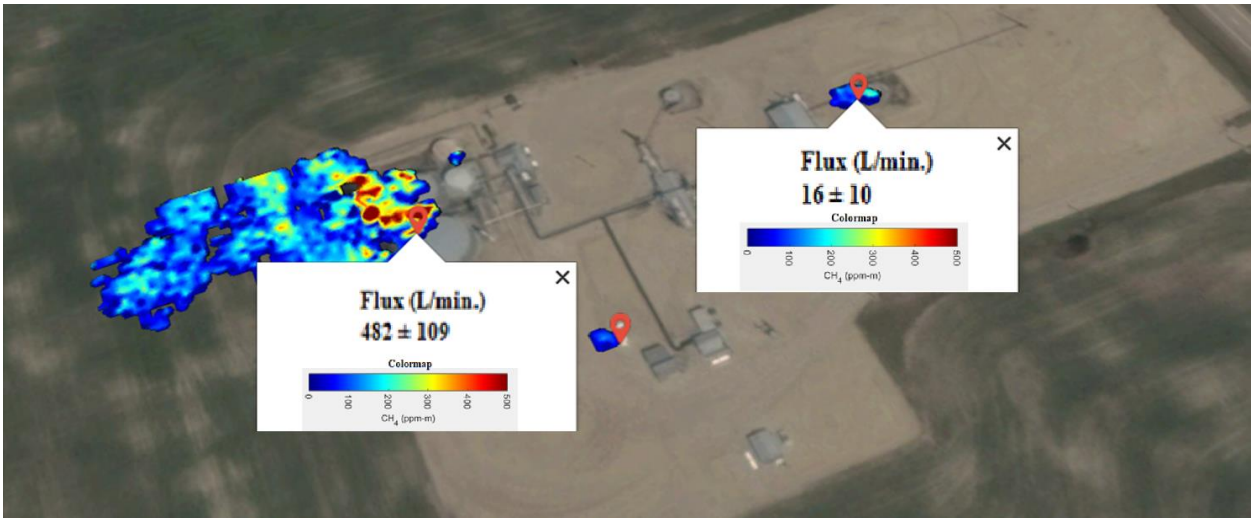

Figure 14. Methane concentration imagery and flux estimates for a complete facility scan of LSD 8-2 acquired on 9/14/2017. In this image the data is displayed using Google Earth. The data is imported using a light weight, easily transmittable .kml file format.

plume shapes to appear in the aggregate images. For the case of the aggregate image in **Figure 14** the wind was consistent across for all flight passes, resulting in consistent looking plumes. In general, there is no requirement to create aggregate facility images from GML because data analysis operations such as concentration mapping, emitter localization and flux quantification computations can be performed on data from a single flight pass. On a separate note, the data presented in **Figure 14** is an overlay of a lightweight .kml file representation of the aggregate methane data from 9/14/2017 LSD 8-2 facility scan in Google Earth. This may be a nice format for transmitting GML data to field operators as it requires no specialized software and complete information about emissions for an entire facility can be transmitted with about 100 kB of data.

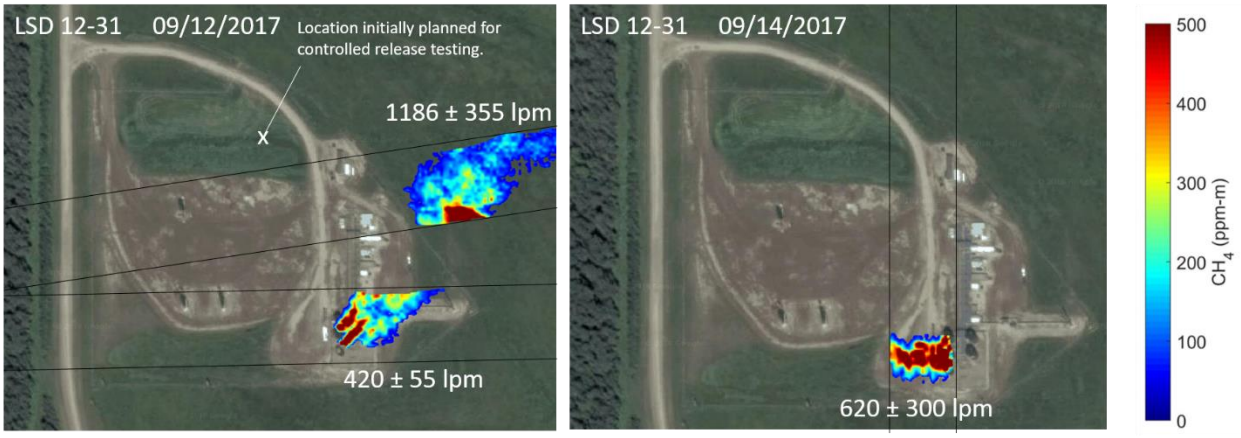

Figure 15. LSD 12-31 facility scan flight passes acquired on 9/12/2017 (left) and 9/14/2017 (right). The black lines indicate the measurement swath for the displayed flight passes, and flux estimates are shown next to each detected plume.

Facility site LSD 12-31, being somewhat larger than LSD 8-2, required a minimum of six flight passes using the prototype GML sensor to acquire a complete facility scan. Two examples of methane concentration maps produced from GML flight passes over LSD 12-31 are shown in **Figure 15**. Much like LSD 8-2,

measurements of this facility revealed large and unanticipated emissions from storage tanks (shown in **Figure 15**) as well as adjacent equipment, including the flare stack (not shown). The emissions measured from the estimated emissions from the storage tank were 420±55 lpm, whereas the downstream emissions, that include contributions from the adjacent equipment were measured by be 1186±355 lpm. The leak measured on LSD 12-31 was so large it interfered with our attempt to perform controlled leak tests on the North end of this facility on 9/12/2017. Shifting winds during the test cause periodic wafting of methane from the infrastructure through the controlled release zone. As a result, we chose to move controlled release testing to the Cooking Lake Site where we could be more confident that nearby methane emissions did not skew our results. The upshot was that we had an anemometer on site for the 12-31 facility scans, and therefore were able to compare flux estimates derived from Meteoblue wind data with those derived from anemometer data. We found good agreement between the flux estimates using the two types of wind data, to within the 1σ measurement uncertainty. That said, so far we only have comparison data for one plume measured at one facility on one day. Much more testing will be

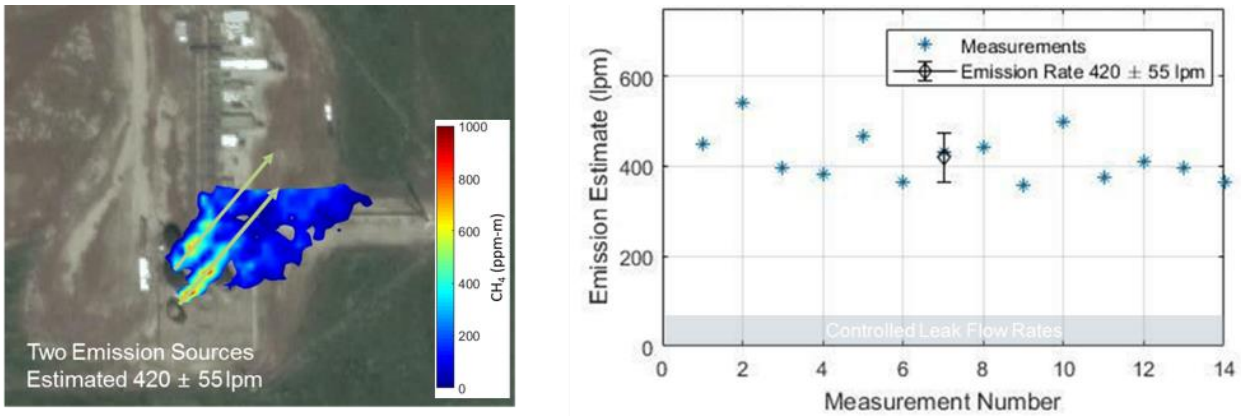

Figure 16. LSD 12-31 uncontrolled emission rate determination performed on 9/12/2017 using on-site anemometer for wind measurement. Left: plume image for LSD 12-31 storage tank emissions. Right: Emission rate estimates derived from the storage tank plume imagery.

required to determine if Meteoblue data is an adequate substitute for local anemometer data for general measurement cases.

The largest facility scanned was 5-30. A minimum of nine flight passes was required to acquire a complete scan of 5-30. This facility was an interesting case because it is 'sour gas' production facility, meaning that the gas composition has a significant component of hydrogen sulfide (H_2S). Due to the H_2S content in the gas, the operators of this facility take extra care to ensure that minimal leakage occurs at this facility due to the health and safety risks posed. GML scans of this facility, shown in **Figure 17**, revealed only one leak present on the site, with a much lower emission rate than the leaks detected at the other two facilities. Additionally, the GML detected a leak at a smaller, adjacent facility that happened to be along one of the flight path lines for the 5-30 facility scan. A zoomed in view of the map at the location of the plume shown in **Figure 17** (left) reveals a single isolated tank which was emitting methane at a rate of 180±69 lpm.

Figure 17. LSD 5-30 facility scan flight passes acquired on 9/14/2017. The black lines indicate the measurement swath for the displayed flight passes, and flux estimates are shown next to each detected plume. The right image shows a leak that was detected on a smaller adjacent facility adjacent during the LSD 5-30 scan.

The final images presented in this section show comparisons of plume images acquired using GML and plume images acquired with a FLIR GasFindIR camera for the same location, not the same time, see **Figures 18 and 19**.

The point of this is to get a feel for the differences between these two gas imaging technologies including the advantages/disadvantages of each. The FLIR GasFindIR camera has the benefit of a fast frame rate and a sensor array, such that it can rapidly acquire image frames and does not require a scanning mechanism for image acquisition. The downsides of the FLIR GasFindIR camera, and other comparable gas cameras, include:

1) IR cameras do not measure gas absorption, but rather temperature differences, making them prone to missed detections and false detection.
2) The detection sensitivity is highly dependent on environmental conditions (e.g. temperature, wind conditions and the type of background behind the gas plume).
3) Plumes detected by IR cameras are not quantitative measurements of gas concentration, which precludes flux determination.

By contrast, the GML directly measures methane concentration and is highly insensitive to environmental conditions, including the properties of the backscatter target. As a result, GML provides high sensitivity detection of regions of anomalous methane concentration with low rates of false detection. This allows users to confidently locate, quantify and prioritize their response to detected methane emissions. Included with this report are FIELD INSPECTION VIDEOS from two of the nominated sites that were surveyed prior to the GML test flights by AER using a FLIR GasFindIR camera.

An interesting note is that during our controlled release tests the low rate emissions of 20 lpm were not visible to the GasFindIR camera, even at very close range and with a solid background set up behind the plume. That the GML sensor was quite able to clearly visualize and map the plume at the same rate from several hundred feet up is a clear indication of the effectiveness of the GML sensor.

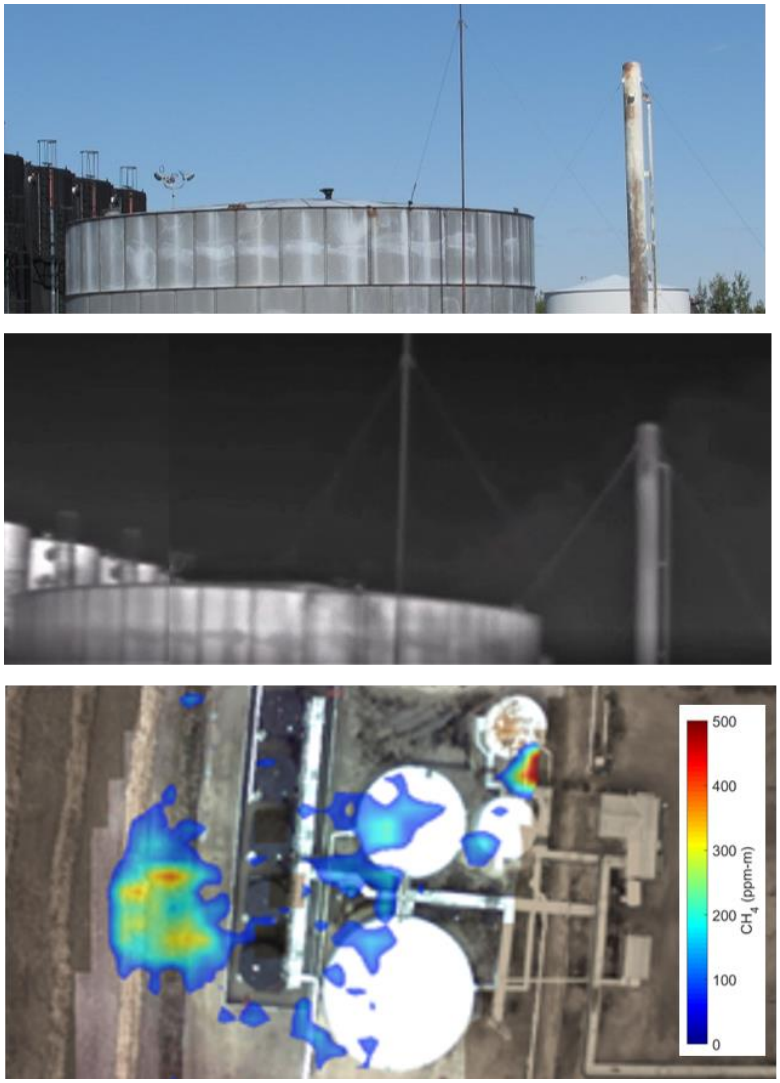

Figure 18. Comparison GML and FLIR GasFindIR images for emissions emanating from LSD 8-2 storage tanks.

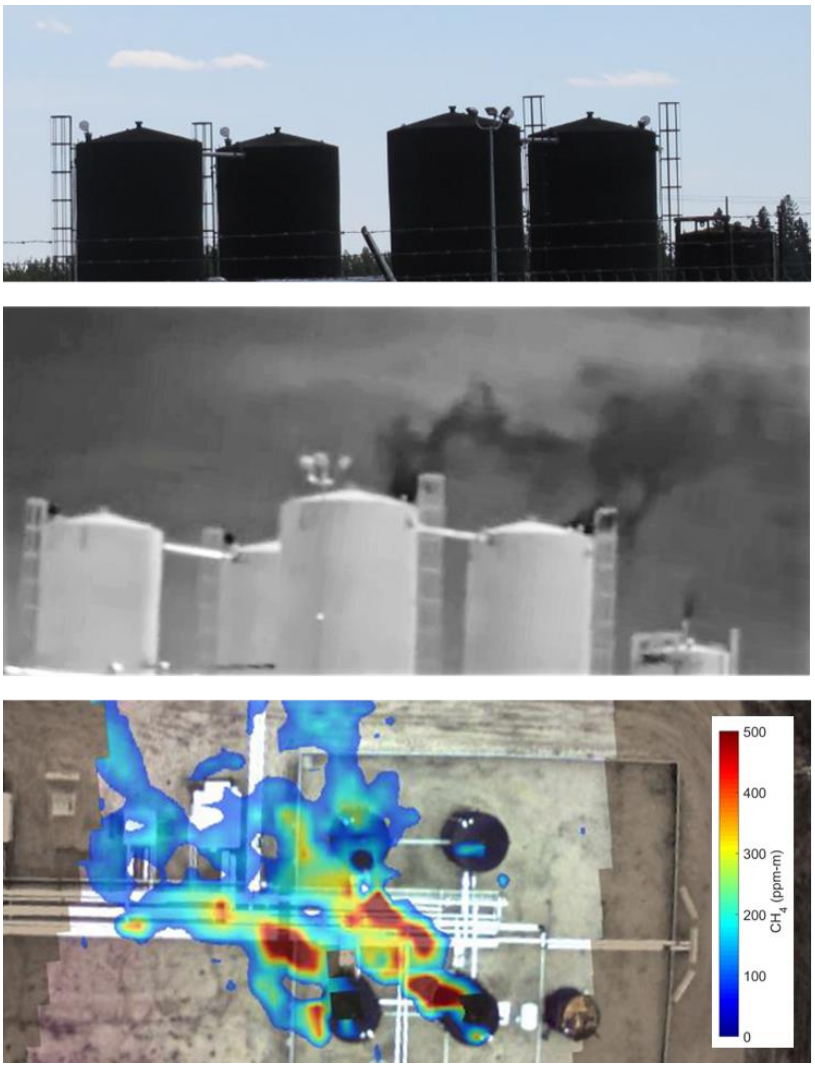

Figure 19. Comparison GML and FLIR GasFindIR images for emissions emanating from LSD 12-31 storage tanks.

5.3 Challenges

We encountered several challenges during the testing period, the first being time constraints. Border crossing issues took up one of the five days scheduled for testing, and bad weather permitted flights on only two of the remaining four days. Despite only having two days to integrate the GML onto the aircraft and perform flight tests we were able to complete five full scans of three different production facilities and perform one full set of controlled release flux measurements.

Additional challenges involving the sensor performance and GML data acquisition from a fixed wing aircraft were also uncovered. The first challenge was related to reliably measuring the intended targets on the ground by flying the plane such that the GML swath covered those targets. Despite being a highly skilled pilot Darryl had difficulty repeatedly placing the GML swath on the intended targets because we were not using autopilot, the plane had some roll instability and the prototype GML had a relatively narrow field of view (18^{o}). To mitigate this issue we attempted to implement survey line navigation using the Pipistrel's autopilot system, but did not get the implementation perfected before the end of the test period. As a result we had to perform a large number of flight passes to map an entire facility. Despite the large number of flight passes some gaps still exist in the facility scan data. We also experienced inefficient acquisition of controlled release data, useful data was extracted from only 28 of the 50 flight passes. LSI will address the flight issues by working out the details of autopilot navigation ahead of future flight tests and investigating aircraft with lower roll instability for future testing. LSI will integrate the GML sensor with LSI's Matrix data acquisition system. LSI's Matrix platform provides an excellent means to leverage pre-existing high-quality and highly-relevant aerial survey systems for the GML sensor. Bridger has addressed the field of view issue in the production GML design that will be available in for testing in May, 2018, by expanding the field of view. The next challenge regarded the GML's FMCW range measurement. Due to greater than expected vibrations during flight, and the method Bridger chose for compensating Doppler shifts on the FMCW range measurements, the range measurement precision was worse than expected. The choice of Doppler compensation scheme also resulted in an effect called 'ghosting' where the same object occasionally appears in two different locations. Bridger's solution for this issue in the production GML design is expected to improve the range measurement precision by a factor of 4 and eliminate occurrences of ghosting. Finally, on the second day of testing (9/14/2017) we uncovered another issue with the GML's FMCW range measurement that was caused by the lower temperature on that day (10^{o}C). When exposed to the colder temperature the FMCW laser control electronics created excess noise that made the range measurement unreliable. The degraded ranging performance was evident just after takeoff, however, the sensor warmed up in route to the test sites, and the facility measurements and controlled release tests performed that day were unaffected. Nonetheless, Bridger has addressed this issue in the production GML design such that GML operation in colder temperatures will be possible, see **Figure 20**.

Parameter	Prototype GML Performance	Expected Production GML Performance
Max measurement distance	230 m	340 m
Measurements per second	10,000 s^{-1}	10,000 s^{-1}
Concentration detection limit	10-15,000 ppm-m (CH_4)	10-15,000 ppm-m (CH_4)
Minimum detectable leak rate (1 m/s wind, 5σ, @max altitude)	10 lpm	10 lpm
Range Precision (1σ)	0.2 m	0.05 m
SW&P	12”x14”x20”, 21 kg, 150 W	11”x11”x20”, 19 kg, 150 W
Ingress protection/Impact rating	IP54	IP65
Operating temperature range	10 °C – 40 °C	-10°C – 50°C

Figure 20. Comparison of prototype GML and production GML performance specifications.

5.4 Safety

No safety related incidents or issues were encountered during the testing period. Standard operations safety practices for field operations of this type were adhered to in conjunction with an Alberta Energy Regulator field inspector and records kept for each day of field operations.

6.0 CONCLUSIONS

Overall, the initial fixed wing GML flight tests went very well. Integration of the GML onto the Pipistrel aircraft was completed in a few hours, and presented no unanticipated surprises. Data acquired from five complete facility scans and the one controlled release test was sufficient to produce a strong initial assessment of GML’s detection sensitivity, concentration mapping capabilities and flux rate quantification performance. Anomalous methane concentrations as low as 25 ppm-m were detectable and locatable with 5σ confidence, and GML demonstrated the ability to quantify emission rates as low as 10 litres/minute. Given the performance improvements Bridger is planning for the first production batch of GML sensors it is likely that GML will be an efficient and cost effective tool for large area leak detection, localization and quantification. In particular, the higher maximum flight altitude and the wider field of view features of the production GML should allow much larger measurement swaths such that even the largest production facilities can be scanned in a few passes, and the smaller ones can be surveyed in a single pass. Further testing will be required to validate the production GML performance upgrades, validate flux measurements in a wide variety of measurement conditions and assess the best sources of wind information for producing flux estimates.

7.0 NEXT STEPS

Further tests providing a broader set of measurements under varying conditions will be useful to better understand the sensor sensitivity in general measurement conditions and to increase both leak detection and quantification confidence.

Continued testing will also be useful to expand our understanding of the conditions under which accurate flux estimates can be made. We had intended to perform more flux testing during our September campaign, but challenging weather conditions limited our testing opportunities.

Specific goals for future tests will include:

1. **Increasing the wind speed range for controlled emission tests:** The data collected in these tests correspond to wind speeds between 0 m/s and 2 m/s. Performing controlled tests in greater wind speed conditions, from 0 m/s to 10 m/s, will be implemented to accommodate the expected range of wind speeds that may be encountered in normal operations.

2. **Estimating flux with different wind data sources:** An onsite anemometer will not always be available to provide local wind data. Bridger is currently working to develop techniques that will enable flux estimates without a local anemometer. Testing and validation of these techniques will be an important step toward a generally applicable approach to flux estimation. These tests may also include the mounting of a research-grade Air Data probe on the aircraft wing for accurate measurements at altitude.

3. **Increasing the GML field of view:** Bridger's first batch of production units will feature a larger field of view, which will make it much easier for pilots to capture the emission source in the GML measurement swath. This will increase the flight efficiency of controlled emission measurement campaigns.

4. **Survey operations system integration:** The extension of the airborne instrumentation to include a high-resolution camera for clear imaging of the terrain and features, a survey-grade GPS/GNSS-Inertial system for accurate geo-positioning of all data and imagery, and the inclusion of a pilot navigation graphics display directly linked to the data collection system, as well as appropriate packaging of these and other components, are all expected to contribute to the optimal field operation of the sensor on an on-going basis.

ACKNOWLEDGEMENTS

LiDAR Services International Inc. would like to state here that the science, capability and "can do" spirit of Dr. Mike Thorpe and Dr. Aaron Kreitinger and the team at Bridger Photonics rendered this successful project possible. The Gas Mapping LiDAR sensor is a proprietary sensor developed by Bridger's team of highly creative innovators. LSI looks forward to a continued working relationship with Bridger Photonics for the promotion of good science and ongoing emissions management operations for the betterment of our planet.

Also, without the forward-thinking support and financial backing of the Alberta Upstream Petroleum Research Fund, the Petroleum Technology Alliance of Canada and their Air Research Planning Committee, and ERA Canada, this project would simply not have been possible. The project team from AER, Suncor, PTAC and AUPRF were all extremely supportive all the way.

Making the world a better place is a team effort and we at LSI are grateful to all involved in bringing attention to the capabilities of the Gas Mapping LiDAR sensor.

Our team:

- Bridger Photonics
  - Mike Thorpe, CTO, PhD
  - Aaron Kreitinger, PhD
  - Peter Roos, CEO, PhD
- LiDAR Services International Inc.
  - Doug Hunter, VP Systems R&D, CET
  - Tony Tubman, President and Managing Director, P.Eng
  - James T Snell, Development Engineer, P.Eng
  - Ryan Burke, Operations Manager, P.Eng
  - Dale Jacobs, Aircraft Fabrication Consultant
- Alberta Energy Regulator (AER)
  - Al Duben, Technical Specialist, Enforcement and Surveillance
  - John Grant, Field Inspector, Enforcement and Surveillance
  - Samantha Clarke, Adviser, Climate Policy Assurance
- Canadian Association of Petroleum Producers (CAPP)
  - Wayne Hillier, Manager, Alberta Operations
- Suncor Energy Services
  - James Beck, Senior Air and Energy Specialist, Environmental Excellence & Climate Strategy
- Petroleum Technology Alliance of Canada (PTAC)
  - Tannis Such, Director, Environmental Research Initiatives
  - Lorie Mayes, Environmental Research Coordinator and Web Site Administrator
  - The PTAC Air Research Planning Committee
- Z-Air Aviation
  - Darryl Zubot, Pilot and Owner

Hats off to everyone else involved directly and indirectly in this project. We at LSI will do our utmost to ensure your efforts were worthwhile.

[i] D.S. Bomse, A.C. Stanton and J.A. Silver, Frequency modulation and wavelength modulation spectroscopies: comparison of experimental methods using a lead-salt diode laser, *Appl. Opt.*, **31**, 718-731 (1992).

[ii] P.A. Roos, R.R. Reibel, T. Berg, B. Kaylor, Z.W. Barber, and W.R. Babbit, Ultrabroadband optical chirp linearization for precision metrology applications, *Opt. Lett*., 34, 3692-3694 (2009).

[iii] B. Galle, et. al. "METHOD FOR MEASURING OF GASEOUS EMISSION AND/OR FLUX." U.S. Patent 6,863,983, issued March 8, 2005.

[iv] https://www.meteoblue.com